Available online at www.sciencedirect.com

SciVerse ScienceDirect

Ceramics International 39 (2013) 4853–4860

CERAMICS INTERNATIONAL

www.elsevier.com/locate/ceramint

Phase formation, dielectric and ferroelectric properties of $Ca_xBa_{1-x}Nb_2O_6$ ceramics

Xiaokun Han, Lingling Wei, Zupei Yang*, Ting Zhang

Key Laboratory for Macromolecular Science of Shaanxi Province, School of Materials Science and Engineering, Shaanxi Normal University, Xi'an, 710062 Shaanxi, PR China

Received 28 September 2012; received in revised form 10 November 2012; accepted 23 November 2012
Available online 20 December 2012

Abstract

Lead-free $Ca_xBa_{1-x}Nb_2O_6$ (CBN, $0.20 \le x \le 0.35$) ceramics were prepared by the conventional solid state method. Effects of Ca content on the phase formation, microstructure, dielectric and ferroelectric properties for the prepared CBN ceramics were systematically studied. XRD results showed that pure CBN phase with tungsten bronze structure could be obtained from the solid solutions of $BaNb_2O_6$ and $CaNb_2O_6$ in all ceramics. Higher Ca contents favored the occurrence of grains with anisometric morphology, but no abnormal grain growth could be found in all compositions. With the increase of x, Curie temperature T_c shifted downward, whereas the maximum dielectric constant ε_m increased initially and then decreased. All the ceramics showed an intermediate relaxor-like behavior between normal and ideal relaxor ferroelectrics according to the modified Curie–Weiss law. Normal ferroelectric hysteresis loops were observed in all compositions. Both remnant polarization P_r and coercive field E_c increased initially and then decreased with the increase of x. The ceramics with homogeneous microstructure, high density and better properties were obtained at $x=0.28$ with $\varepsilon_m=2998$, $T_c=234$ °C, $P_r=3.98$ μC cm^{-2} and $E_c=14.03$ kV cm^{-1}.

Keywords: B. X-ray methods; C. Dielectric properties; D. Niobates; Tungsten bronze structure

1. Introduction

As one member of the lead-free ferroelectric systems, tungsten bronze compounds have received considerable attention due to their superior electro-optic, dielectric, ferroelectric and pyroelectric properties [1–3]. Formally, the tungsten bronze (TB) structure can be developed from the perovskite type structure by tilting the oxygen octahedral in the way to form a lattice with three different types of voids. TB structure has a chemical formula of $(A1)_2(A2)_4(C)_4(B)_{10}O_{30}$, where A type of cations (Sr^{2+}, Ba^{2+}, Ca^{2+}, Pb^{2+}, K^+, Na^+ and some rare earth cations) occupy A1 and A2 sites, while B type of cations (Nb^{5+}, Ta^{5+}) occupy the B octahedral sites, and the C sites are occupied by Li^+ and other small cations. The polar unit of tungsten bronze niobate compounds is the Nb_2O_6 octahedron. Tungsten bronze solid solutions can be obtained with either tetragonal symmetry in ferroelectric phase or orthorhombic symmetry in both ferroelectric and ferroelastic phases. Ferroelectricity in these compounds derives from the interaction between the Nb atoms and the oxygen framework in the polar unit [4–6].

As one typical promising material of TB compounds, $Sr_{1-x}Ba_xNb_2O_6$ (SBN) has been studied intensively because of its outstanding physical properties such as large electro-optic and pyroelectric coefficients [7,8]. SBN is the solid solutions of $SrNb_2O_6$ and $BaNb_2O_6$, and the TB phase can be obtained in a wide range of compositions with $0.25 \le x \le 0.75$. Great efforts have been devoted to the SBN ceramics with $x=0.53$ since they show improved electrical properties [9]. However, the low Curie temperature T_c of about 80 °C limits its widespread applications. In addition, abnormal grain growth and duplex structure are frequently encountered in SBN ceramics, which significantly deteriorates their electrical properties [10]. $Ca_xBa_{1-x}Nb_2O_6$ compound (CBN, which was first mentioned as a ceramic material in 1959 by Iszmailzade [11]) is

*Corresponding author. Tel.: +86 29 81530 718; fax: +86 29 81530 702.
E-mail address: yangzp@snnu.edu.cn (Z. Yang).

0272-8842/$ - see front matter © 2012 Elsevier Ltd and Techna Group S.r.l. All rights reserved.
http://dx.doi.org/10.1016/j.ceramint.2012.11.078

the Ca analog of SBN. Contrary to Sr in SBN, the smaller Ca ions in CBN can only occupy A1 sites of the two large A sites in the tungsten bronze framework of NbO_6 octahedral. The main advantage of CBN compound is the high Curie temperature in the range of 250–280 °C, almost 200 °C higher than that of SBN. In recent years, CBN compounds have received increasing interests, in which most works are mainly focused on the single crystals and thin films [12–15]. However, applications of single crystals with excellent electric properties are limited by their high cost and difficulty in fabrication. In comparison, ceramics can be fabricated into larger and more complex components at lower cost. However, the microstructure and electrical properties of CBN ceramics with different Ca contents have not yet been well explored.

In this work, the $Ca_xBa_{1-x}Nb_2O_6$ ceramics were prepared by the conventional mixed-oxide method. Effects of Ca content on phase formation, microstructure, dielectric and ferroelectric properties of CBN ceramics were experimentally studied and systematically investigated. In addition, the correlation between the structure and electrical properties of CBN ceramics with different Ca contents was demonstrated.

2. Experimental

A conventional mixed-oxide technique was used to prepare the samples with compositions of $Ca_xBa_{1-x}Nb_2O_6$ ($x=0.20$, 0.22, 0.28, 0.30, 0.35 and 0.38). The starting powders were reagent grade $BaCO_3$, $CaCO_3$, and Nb_2O_5 as received. They were weighed and ball-milled for 16 h with agate media in alcohol, then dried and calcined at 1150–1225 °C for 4 h. The calcined powders were mixed with 5 wt% polyvinyl alcohol (PVA) solution and then pressed into pellets with a diameter of 1.5 cm under 300 MPa pressure. After burning out the PVA, the green samples were sintered in air at selected temperatures for 4 h.

The structure of the ceramic samples was analyzed by x-ray diffraction (XRD, D/max-2200, Rigaku, Tokyo, Japan). Microstructure evolution was observed using a scanning electron microscopy (SEM, Model Quanta 200, FEI Company, Eindhoven, Netherlands). Silver electrodes were formed on both surfaces of each sintered disk by firing silver at 840 °C for 30 min. Weak-field dielectric response was measured by a LCR meter (Agilent 4284A) with a four-wire probe and a signal level of 1 V/mm, in a frequency range of 1–1 MHz. Samples were measured from room temperature to 420 °C and subsequently cooling down to room temperature again at a heating or cooling rate of 2 °C/min. The polarization versus electrical (P–E) hysteresis loops were carried out by a Radiant Precision Workstation (Albuquerque, NM, USA).

3. Results and discussion

XRD patterns of $Ca_xBa_{1-x}Nb_2O_6$ (CBN) powders prepared at different conditions are shown in Fig. 1. Fig. 1(a) shows the XRD patterns of CBN powders with different x ($x=0.20$, 0.22, 0.25, 0.28, 0.30, 0.35) calcined at the same temperature of 1200 °C. As shown in Fig. 1(a), when the calcining temperature is 1200 °C, only the samples with $x=0.25$ and 0.28 show pure CBN phase with TB structure. The $BaNb_2O_6$ impurity phase indicated by diamond label at $2\theta=28.3^\circ$ is observed in Ba-rich samples with $x=0.20$ and 0.22 (JCPDS card #32-0077). And the $CaNb_2O_6$ impurity phase indicated by asterisk label at $2\theta=23.6^\circ$ is observed in Ca-rich samples with $x=0.30$ and 0.35 (JCPDS card #39-1392). In order to further study the phase formation process of CBN phase, the XRD patterns of CBN powders with $x=0.20$, 0.28 and 0.30 calcinated at different temperatures were shown in Fig. 1(b), (c) and (d), respectively. It can be seen that at the calcining temperature of 1150 °C, both $BaNb_2O_6$ and $CaNb_2O_6$ phases are detected for all samples with $x=0.20$, 0.28 and 0.30. According to Fig. 1(b) and (d), with the increase of calcining temperature, the intensities of the XRD peaks at $2\theta=23.6^\circ$ and $2\theta=28.3^\circ$ associated to the two impurity phases decrease gradually, and disappear completely when the calcining temperature is 1225 °C, demonstrating that pure CBN phase can be obtained at higher temperature of 1225 °C for samples with $x=0.20$ and 0.30. However, the CBN phase formation temperature for sample with $x=0.28$ is 1200 °C (Fig. 1a and c), indicating that the CBN phase formation for the sample with $x=0.28$ is the easiest in all the samples. Both $BaNb_2O_6$ and $CaNb_2O_6$ are considered as the intermediate products to form the final CBN phase. And the detailed reaction equations can be concluded as follows:

(1) $BaCO_3+Nb_2O_5\rightarrow BaNb_2O_6+CO_2$
(2) $CaCO_3+Nb_2O_5\rightarrow CaNb_2O_6+CO_2$
(3) $xCaNb_2O_6+(1-x)BaNb_2O_6\rightarrow Ca_xBa_{1-x}Nb_2O_6$

The intermediate products $BaNb_2O_6$ and $CaNb_2O_6$ form directly from the raw materials, and then the CBN phase is obtained from the solid solutions of $BaNb_2O_6$ and $CaNb_2O_6$. Fig. 2 shows the XRD patterns of CBN ceramics with different x sintered at the same temperature of 1340 °C. It can be seen that all ceramics have single TB structure and no evidence for second phase, showing that pure CBN phase with TB structure can be obtained in ceramics form at the region of $0.20\le x\le 0.35$. It has been reported that the TB structure with a unit-cell formula of $(A1)_2(A2)_4(C)_4(B)_{10}O_{30}$ consists of a framework of NbO_6 octahedra, and three different types of interstitial sites (A1, A2, and C sites). For CBN compounds, the relative smaller Ca^{2+} ions (1.34 Å) occupy only the 12-fold coordinated oxygen octahedral A1 sites, while the bigger Ba^{2+} ions (1.47 Å) occupy the residual A1 sites and 15-fold coordinated oxygen octahedral A2 sites. Muehlberg reported that the eutectic lines with the stability region of CBN was found to be $0.15\le x\le 0.40$, and retrograde solubility lines limited the stability region to $0.17\le x\le 0.33$ [16]. The x region chosen in this work ($0.20\le x\le 0.35$) locates

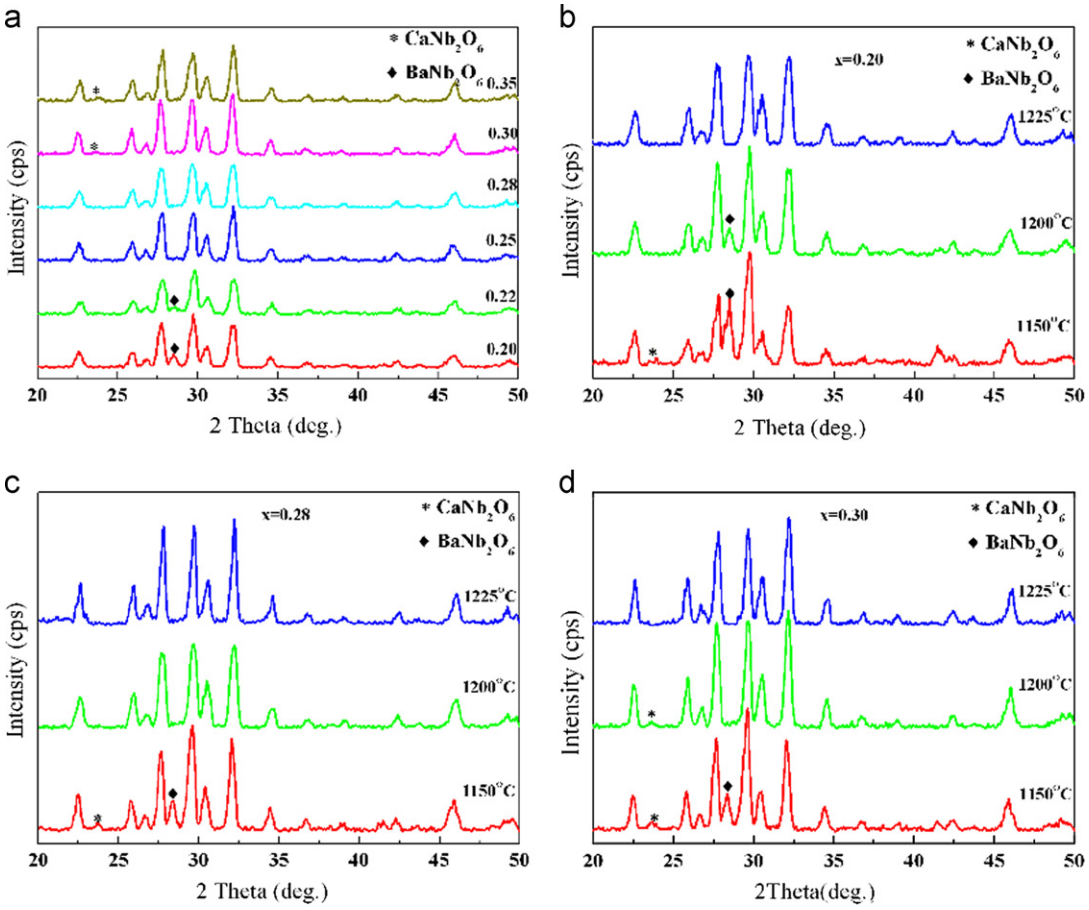

Fig. 1. XRD patterns of CBN powders prepared at different conditions: (a) XRD patterns of CBN powders calcined at 1200 °C with different x; (b) XRD patterns of CBN powders with $x=0.20$ calcined at different temperatures; (c) XRD patterns of CBN powders with $x=0.28$ calcined at different temperatures; (d) XRD patterns of CBN powders with $x=0.30$ calcined at different temperatures.

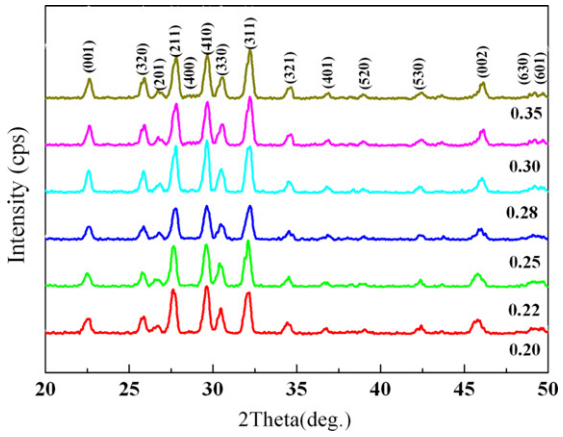

Fig. 2. XRD patterns of CBN ceramics sintered at 1340 °C with different x.

in the eutectic stability region of $0.15 \leq x \leq 0.40$, then it is reasonable that pure CBN phase can be obtained in all samples. In addition, it can also be concluded that the lattice is distorted least at $x=0.28$ and the solid solution of $Ca_{0.28}Ba_{0.72}Nb_2O_6$ sample has the best stability in all the samples, as the CBN phase formation is the easiest at $x=0.28$.

Fig. 3 shows the SEM images of the CBN ceramics with different x sintered at the same temperature of 1340 °C. It is found that the ceramics with homogenous microstructure can be obtained when $x=0.20$ and 0.22. At $x=0.25$, most of the grains show equiaxed morphology, while very little anisometric pillar-type grains can also be found in Fig. 3(c). This phenomenon also exists in CBN ceramics with $x>0.25$. It is obvious that the proportion of anisometric pillar-type grains increases with the increase of x. The occurrence of anisometric morphology may be attributed to the growth habit of TB structure, for which the grain growth in (001) facet is faster due to the lower surface energy [17]. The pillar-type grains were also found in CBN compounds by Shanmingke who claimed that this pillar-type grain growth might be caused by a mechanism of partial melting [18]. Higher Ca contents are beneficial to the partial liquid formation at the sintering process. Then the mass transport takes place by diffusion of ions to the growing steps through the fluid phase rather than fusion of adjacent grains. In addition, abnormal grain growth (>50 μm) encountered frequently in SBN ceramics cannot be observed in any of the CBN specimens. According to Lee and Freer [10], for SBN ceramics, the liquid phase

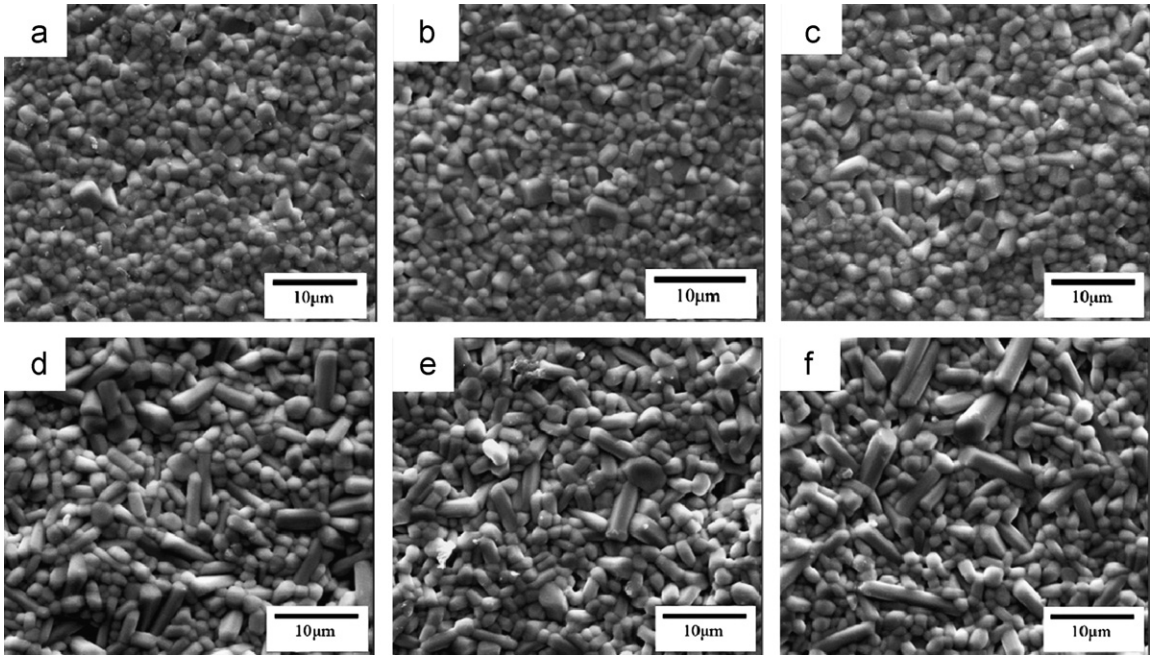

Fig. 3. Scanning electron microscopy photographs of the surface of CBN ceramics with different x: (a) $x=0.20$; (b) $x=0.22$; (c) $x=0.25$; (d) $x=0.28$; (e) $x=0.30$; and (f) $x=0.35$.

resulting from locally inhomogeneous compositions due to partially uncompleted calcination will lead to the formation of abnormal grain growth. In this work, the CBN powders used to fabricate ceramics are all of single TB phase which prevents effectively the growth of abnormal grain.

Fig. 4 shows the relative density of the CBN ceramics with different x sintered at 1340 °C. The relative density is calculated based on the theoretical density of CBN28 (5.334 g cm^{-3}) [19]. The relative density increases gradually with increasing x, and reaches the maximum value of about 98.5% at $x=0.28$, and then decreases. Combining with the results of SEM micrographs, it can be concluded that when $x>0.28$, the amounts of anisometric grains increase, leading to higher porosity and lower density. The differences between the stoichiometric and microstructural characterizations are likely to have substantial influence on the electrical properties, and then the effects of Ca contents on electrical properties are also studied and discussed in the following sections.

Fig. 5 shows the temperature dependence of dielectric constant ε and dielectric loss tan δ for the CBN ceramics with different Ca contents. The dielectric constant ε for all specimens increases with the increase of measuring temperature, and then decreases after reaching a maximum value. The peaks of ε are associated to the ferroelectric to paraelectric phase transition. Moreover, the dielectric characteristics show diffuse phase transition (DPT) phenomena (exhibit a broad Curie peak in the phase transition range) for each composition. The position of the dielectric constant peak shifts toward higher temperatures with increasing the frequency, which could be attributed to the ion disorder in the unit cell. The variations of tan δ

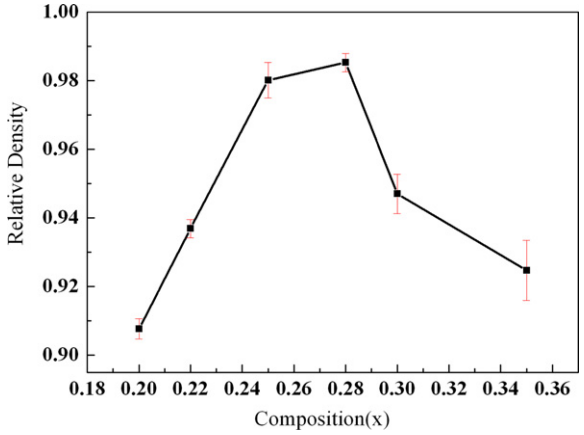

Fig. 4. Relative density of CBN ceramics sintered at 1340 °C with different x.

with temperature for all ceramics show similar trend. All of the samples show tan δ peaks below the phase transition temperature (T_c). This phenomenon is generally observed in ferroelectrics and can be attributed to the improvement of the domain wall during the ferroelectric to paraelectric phase transition [20,21]. It is well known that dielectrics loss is a sum of the resistive loss and the relaxation loss of the dipoles [22]. The relaxation loss comes from relaxation of the dipoles which expends energy and the resistive loss comes from energy spent by free carriers due to the oxygen vacancies [23]. The decrease of tan δ value above T_c can be a consequence of decrease in relaxation time with temperature [23]. This decrease in relaxation time allows dipoles to be in company with the applied electric field so lowers the tan δ. It is also observed that the values of tan δ

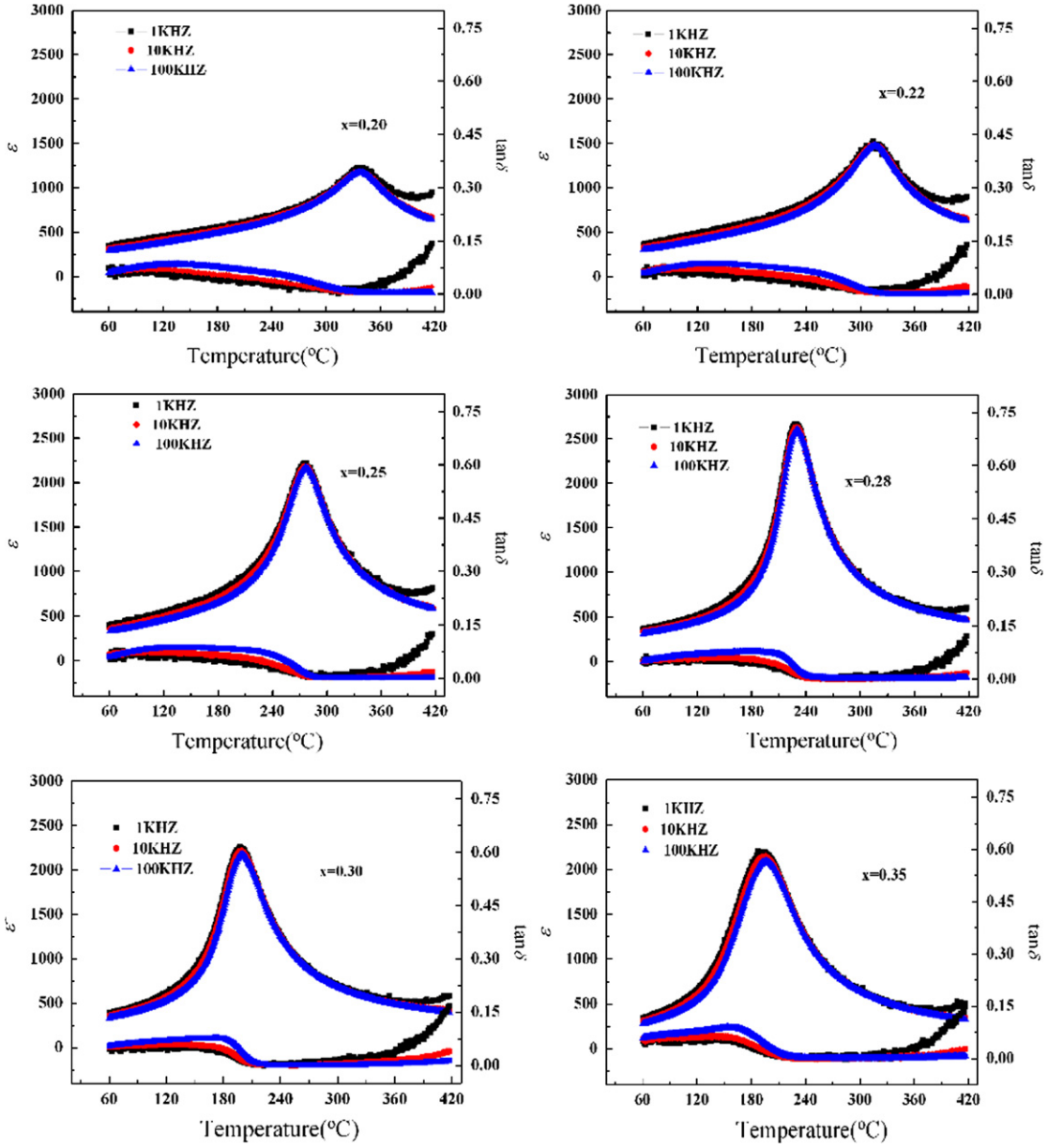

Fig. 5. The temperature dependence of dielectric constant ε and dielectric loss tan δ for CBN ceramics with different x measured at different frequencies.

at high frequencies are much lower compared with those at low frequencies. This kind of dependence of tan δ on frequency is typically associated with a loss of energy by the conduction process.

Fig. 6 shows the temperature dependence on ε for CBN ceramics measured at 1 kHz as a function of x. ε_m is the maximum value of dielectric constant obtained at the phase transition temperature (T_c). As shown in Fig. 6(a), the position of phase transition shifts to lower temperatures, while ε_m increases initially and then decreases with increasing x. Fig. 6(b) shows ε_m and T_c for the ceramics with different Ca contents measured at 1 KHz frequency. ε_m increases initially from 1630 at $x=0.20$ to 2998 at $x=0.28$, then decreases with further increasing x above 0.30. In addition, T_c decreases gradually from 338 °C to 190 °C as increasing x from 0.20 to 0.35. The dielectric behavior of the $Ca_xBa_{1-x}Nb_2O_6$ ceramics sintered at 1340 °C can also be explained by the modified Curie–Weiss law: $1/\varepsilon-1/\varepsilon_m=(T-T_m)^\gamma/C$, where ε_m is the maximum value of the dielectric constant, T_m is the temperature at which ε reaches the maximum value, γ and C are assumed to be constants. The limiting value $\gamma=2$ allows the equation to fit the conventional Curie–Weiss law valid for the normal ferroelectric, and $\gamma=1$ allows the equation to fit the quadratic valid for an ideal relaxor ferroelectric. When γ is between 1 and 2, it means a so-called incomplete diffuse phase transition. The values of γ for the $Ca_xBa_{1-x}Nb_2O_6$ ceramic at 1 kHz were obtained from the slopes of $\ln[(\varepsilon_m/\varepsilon)-1]$ versus $\ln(T-T_m)$ plots in Fig. 7. The γ value varies between 1.32 and 1.83 at different

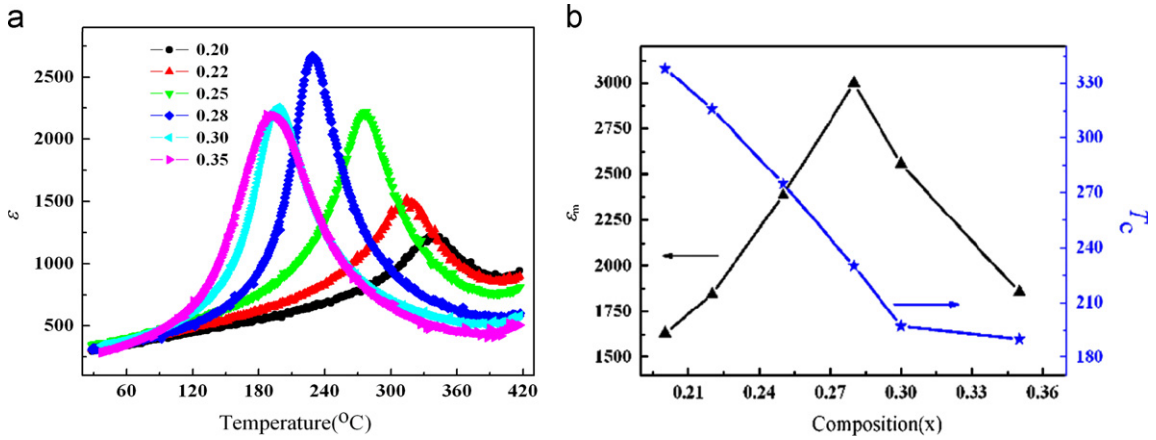

Fig. 6. The dielectric properties of CBN ceramics: (a) Temperature dependence of ε for CBN ceramics measured at 1 kHz as a function of x; (b) ε_m and T_c of the CBN ceramics measured at 1 kHz as a function x.

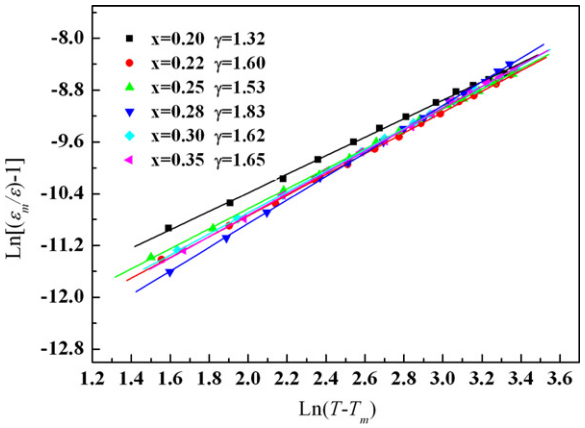

Fig. 7. $\ln[(\varepsilon_m/\varepsilon)-1]$ as a function of $\ln(T-T_m)$ for the CBN ceramics with different x.

x, indicating that all the ceramics show intermediate relaxor-like behavior between normal and ideal relaxor ferroelectrics.

The polarization levels versus applied electrical field (P–E) hysteresis loops for all samples measured at room temperature are shown in Fig. 8(a). It can be seen that all samples show unclosed hysteresis loops, and the P–E hysteresis loops become relatively saturated as x increases from 0.20 to 0.28. When further increasing x, the P–E hysteresis loops become slimmer. As shown in Fig. 8(b), the $Ca_{0.28}Ba_{0.72}Nb_2O_6$ ceramics exhibit higher P_r (3.98 μC cm^{-2}) and a relatively lower E_c (14.03 kV cm^{-1}). P_r of the ceramics with $x>0.28$ becomes much lower. In addition, with increasing x, E_c increases at first, reaches the maximum value of 16.75 kV cm^{-1} at $x=0.25$ and then gradually decreases, indicating that the ceramics with $x>0.25$ are easiest to be poled.

According to the above results, the ceramics with optimized dielectric and ferroelectric properties are obtained at $x=0.28$, which is in accordance with the result of CBN single crystals [24]. The P–E hysteresis loops, P_r and E_c measured at different temperatures in silicon oil for the

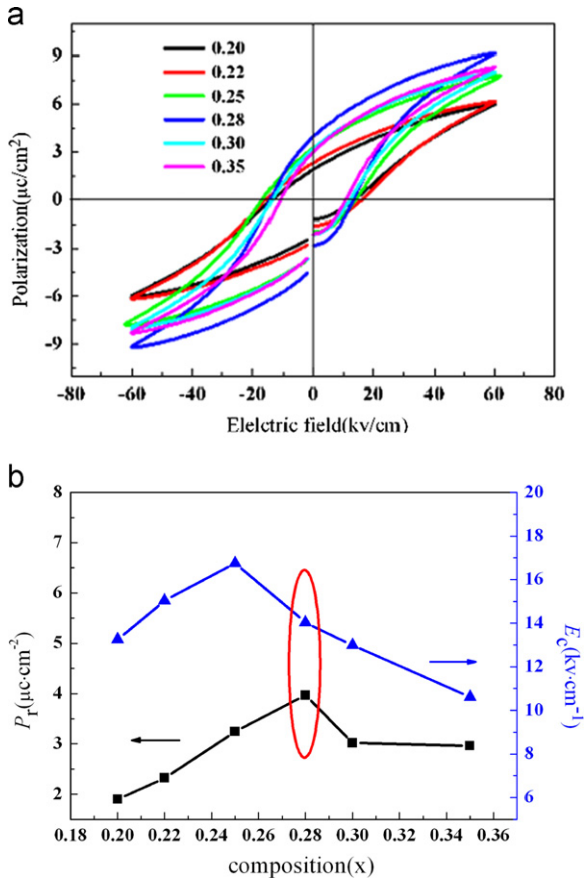

Fig. 8. The ferroelectric properties of CBN ceramics with different x measured at room temperature: (a) P–E hysteresis loops of the CBN ceramics with different x; (b) P_r and E_c of the CBN ceramics as a function of x.

ceramics with $x=0.28$ are shown in Fig. 9. P–E hysteresis loops are less predominant at higher temperatures, and higher temperatures lead to the constriction in the loops (Fig. 9a). P_r and E_c in all samples decrease but not vanish with increasing the temperature from 25 °C to 125 °C (Fig. 9b). The similar trend is also observed in lead-based ceramics and other lead-free ceramics [25,26].

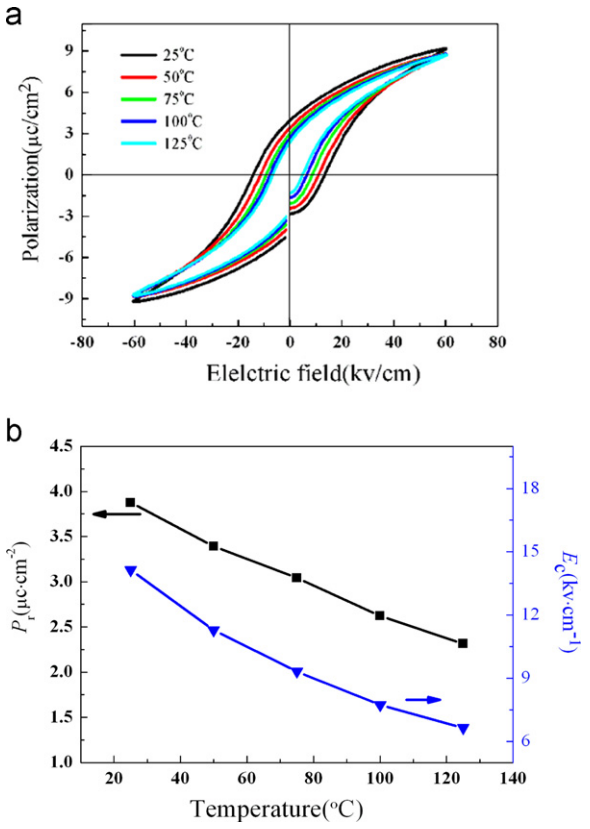

Fig. 9. The ferroelectric properties of CBN ceramic with $x=0.28$ measured at different temperatures: (a) P–E hysteresis loops of the $Ca_{0.28}Ba_{0.72}Nb_2O_6$ ceramics; (b) P_r and E_c of the $Ca_{0.28}Ba_{0.72}Nb_2O$ ceramics measured at different temperatures.

4. Conclusions

Tungsten bronze structure $Ca_xBa_{1-x}Nb_2O_6$ ceramics ($x=0.20$, 0.22, 0.25, 0.28, 0.30 and 0.35) were prepared by the conventional mixed-oxide method. The phase structure, microstructure, dielectric properties and ferroelectric properties of prepared ceramics as a function of Ca content were investigated. The XRD results showed that pure CBN phase with tungsten bronze structure could be obtained from the solid solutions of $BaNb_2O_6$ and $CaNb_2O_6$ in all ceramics. The solid solution of $Ca_{0.28}Ba_{0.72}Nb_2O_6$ sample shows the best stability because the CBN phase formation was the easiest at $x=0.28$. Higher Ca contents could lead to the occurrence of grains with anisometric morphology, but no abnormal grain growth could be found in all compositions. The dielectric characteristics showed diffuse phase transition phenomena for all samples, which was proved by linear fitting of modified Curie–Weiss law. The electrical properties of $Ca_xBa_{1-x}Nb_2O_6$ ceramics were significantly depended on x. With increasing x, ε_m increased from 1630 to 2998 and then decreased, and the transition temperature T_c decreased gradually from 338 °C to 190 °C. In addition, both remnant polarization (P_r) and coercive field (E_c) decreased initially and then increased with increasing x. The ceramics with homogeneous microstructure and high density were obtained at $x=0.28$, resulting in the optimized properties: $\varepsilon_m=2998$, $T_c=234$ °C, $P_r=3.98$ μC cm^{-2}, and $E_c=14.03$ kV cm^{-1}.

Acknowledgments

This work was supported by the National Science Foundation of China (NSFC) (Grant no. 51172136), the Fundamental Research Funds for the Central Universities (Program no. GK201101004) and Open Fund of Shaanxi Province Key Laboratory (Program no. 2010SYS-07).

References

[1] R. Neurgaonkar, J.R. Oliver, W.K. Copy, L.E. Cross, D. Viehland, Piezoelectricity in tungsten bronze crystals, Ferroelectrics 160 (1994) 265–276.
[2] K. Kakimoto, T. Yoshifuji, H. Ohsato, Densification of tungsten–bronze $KBa_2Nb_5O_{15}$ lead-free piezoelectric ceramics, Journal of the European Ceramic Society 27 (2007) 4111–4114.
[3] X. Hao, Y.F. Yang, The dielectric and ferroelectric properties of tungsten bronze ferroelectric $(K_{0.5}Na_{0.5})_{0.1}(Sr_{0.5}Ba_{0.5})_{0.95}Nb_2O_6$ (SBN40) ceramic, Journal of Materials Science 42 (2007) 3276–3279.
[4] R.J. Xie, Y. Akimune, Lead-free piezoelectric ceramics in the $(1-x)Sr_2NaNb_5O_{15}-xCa_2NaNb_5O_{15}$ ($x=0.05-0.35$) system, Journal of Materials Chemistry 12 (2002) 3156–3161.
[5] R.J. Xie, Y. Akimune, K. Matsuo, T. Sugiyama, N. Hirosaki, T. Sekiya, Dielectric and ferroelectric properties of tetragonal tungsten bronze $Sr_{2-x}Ca_xNaNb_5O_{15}$ ($x=0.05-0.35$) ceramics, Applied Physics Letters 80 (2002) 835–837.
[6] L.L. Wei, Z.P. Yang, R. Gu, H.M. Ren, The phase formation, microstructure and electric properties of tungsten bronze ferroelectric $Sr_2NaNb_5O_{15}$ ceramics, Journal of the American Ceramic Society 93 (2010) 1984–1990.
[7] P.B. Jamieson, S.C. Abrahams, J.L. Bernstein, Ferroelectric tungsten bronze-type crystal structures. I. Barium strontium niobate $Ba_{0.27}Sr_{0.75}Nb_2O_{5.78}$, The Journal of Chemical Physics 48 (1968) 5048–5057.
[8] E.L. Venturini, E.G. Spencer, P.V. Lenzo, A.A. Ballman, Refractive indices of strontium barium niobate, Journal of Applied Physics 39 (1968) 334–343.
[9] Z.P. Yang, R. Gu, Phase formation, microstructure and dielectric properties of $Sr_{0.53}Ba_{0.47}Nb_{2-x}Ta_xO_6$ ceramics, Journal of Alloys and Compounds 504 (2010) 211–216.
[10] H.Y. Lee, R. Freer, The mechanism of abnormal grain growth in $Sr_{0.6}Ba_{0.4}Nb_2O_6$ ceramics, Journal of Applied Physics 81 (1997) 376–382.
[11] I.G. Iszmailzade, Kristallografiya 5 (1960) 268.
[12] E. Mortazy, I. Stateikina, Low-loss $Ca_xBa_{1-x}Nb_2O_6$ ridge waveguide for electro-optic devices, Microelectronic Engineering 88 (2011) 218–221.
[13] Y.J. Qi, C.J. Lu, Ferroelectric and dielectric properties of $Ca_{0.28}Ba_{0.72}Nb_2O_6$ single crystals of tungsten bronzes structure, Applied Physics Letters 87 (2005) 082904.
[14] W.L. Gao, H.J. Zhang, Growth, electromechanical, and electro-optic properties of tungsten bronze $(Ca_{0.28}Ba_{0.72})_{0.25}(Sr_{0.6}Ba_{0.4})_{0.75}Nb_2O_6$ single crystal, Journal of Applied Physics 107 (2010) 094101.
[15] I. Stateikina, E. Mortazy, S. Delprat, Fabrication of a silicon-based $Ca_xBa_{1-x}Nb_2O_6$ ridge waveguide for electro-optical phase modulation, Semiconductor Science and Technology 25 (2010) 115005.
[16] M. Muehlberg, M. Burianek, Phase equilibrium, crystal growth and characterization of the novel ferroelectric tungsten bronzes $Ca_xBa_{1-x}Nb_2O_6$ (CBN) and $Ca_xSr_yBa_{1-x-y}Nb_2O_6$ (CSBN), Journal of Crystal Growth 310 (2008) 2288–2294.

[17] A.M. Glass, Investigation of the electrical properties of $Sr_{1-x}Ba_xNb_2O_6$ with special reference to pyroelectric detection, Journal of Applied Physics 40 (1969) 4699–4713.

[18] S. Ke, H. Fan, H. Huang, Dielectric, ferroelectric properties, and grain growth of $Ca_xBa_{1-x}Nb_2O_6$ ceramics with tungsten–bronzes structure, Journal of Applied Physics 104 (2008) 024101.

[19] M. Eßer, M. Burianek, Single crystal growth of the tetragonal tungsten bronze $Ca_xBa_{1-x}Nb_2O_6$ (x=0:28; CBN-28), Journal of Crystal Growth 240 (2002) 1–5.

[20] Y.N. Wang, Y.N. Huang, Mechanical and dielectric loss related to ferroelectric and relaxor phase transitions and domain walls, Journal of Alloys and Compounds 211–212 (1994) 356–360.

[21] L.N. Kamysheva, S.N. Rozhdin, The peculiarities of the electrophysical properties of the potassium dihydrogen phosphate (KDP) group crystals connected with the domain structure dynamics, Ferroelectrics 71 (1987) 281–296.

[22] P. Li, J.F. McDonald, T.M. Lu, Densification induced dielectric properties change in amorphous barium titanate thin films, Journal of Applied Physics 71 (1992) 5596–5600.

[23] K. Kumar, B.K. Singh, M.K. Gupta, N. Sinha, B. Kumar, Enhancement in dielectric and ferroelectric properties of lead free $Bi_{0.5}(Na_{0.5}K_{0.5})_{0.5}TiO_3$ ceramics by Sb-doping, Ceramics International 37 (2011) 2997–3004.

[24] Y.J. Qi, C.J. Lu, J. Zhu, Ferroelectric and dielectric properties of $Ca_{0.28}Ba_{0.72}Nb_2O_6$ single crystals of tungsten bronzes structure, Applied Physics Letters 87 (2005) 082904.

[25] X.F. Long, Z.G. Ye, Relaxor behavior in the solid solution between dielectric $Ba(Mg_{1/3}Nb_{2/3})O_3$ and ferroelectric $PbTiO_3$, Applied Physics Letter 90 (2007) 112905.

[26] Z.J. Wang, X.Z. Li, X.F. Long, Z.G. Ye, Characterization of relaxor ferroelectric behavior in the $(1-x)Ba(Yb_{1/2}Nb_{1/2})O_3$–$xPbTiO_3$ solid solution, Scripta Materialia 60 (2009) 830.